Received: 10 August 2020 | Accepted: 22 September 2020
DOI: 10.1002/hyp.13919

SCIENTIFIC BRIEFING

HP TODAY WILEY

Refining image-velocimetry performances for streamflow monitoring: Seeding metrics to errors minimization

Alonso Pizarro[1] | Silvano Fortunato Dal Sasso[1] | Salvatore Manfreda[2]

[1]Department of European and Mediterranean Cultures: Architecture, Environment and Cultural Heritage (DICEM), University of Basilicata, Matera, Italy

[2]Department of Civil, Architectural and Environmental Engineering, University of Naples Federico II, Naples, Italy

Correspondence
Alonso Pizarro, Department of European and Mediterranean Cultures: Architecture, Environment and Cultural Heritage (DICEM), University of Basilicata, 75100 Matera, Italy.
Email: alonso.pizarro@unibas.it

Funding information
European Cooperation in Science and Technology, Grant/Award Number: CA16219

Abstract

River streamflow monitoring is currently facing a transformation due to the emerging of new innovative technologies. Fixed and mobile measuring systems are capable of quantifying surface flow velocities and discharges, relying on video acquisitions. This camera-gauging framework is sensitive to what the camera can "observe" but also to field circumstances such as challenging weather conditions, river background transparency, transiting seeding characteristics, among others. This short communication paper introduces the novel idea of optimizing image velocimetry techniques selecting the most informative sequence of frames within the available video. The selection of the optimal frame window is based on two reasonable criteria: (a) the maximization of the number of frames, subject to (b) the minimization of the recently introduced dimensionless seeding distribution index (SDI). SDI combines seeding characteristics such as seeding density and spatial clustering of tracers, which are used as a proxy to enhance the reliability of image velocimetry techniques. Two field case studies were considered as a proof-of-concept of the proposed framework, on which seeding metrics were estimated and averaged in time to select the proper application window. The selected frames were analysed using LSPIV to estimate the surface flow velocities and river discharge. Results highlighted that the proposed framework might lead to a significant error reduction. In particular, the computed discharge errors, at the optimal portion of the footage, were about 0.40% and 0.12% for each case study, respectively. These values were lower than those obtained, considering all frames available.

KEYWORDS
discharge, fluvial monitoring, hydrometry, large-scale particle image velocimetry, optimization, seeding distribution index, seeding metrics, streamflow velocity

1 | INTRODUCTION

Fluvial monitoring is crucial for water resources policy and management, design of infrastructure such as bridges and dams, development and improvement of hydraulic and hydrological models, and their calibration and validation under different circumstances (Manfreda, Link, & Pizarro, 2018; Owe, 1985). Standard approaches for river streamflow monitoring are invasive and generally based on the use of flow metres or acoustic Doppler current profiles (ADCPs) (Rehmel, 2007; Tazioli, 2011; World Meteorological Organization (WMO), 2010; Yorke & Oberg, 2002). Several drawbacks are unfortunately associated to the use of this standard approach, among them: (a) intrusive modality which may alter flow velocity patterns; (b) the necessity of specialized operators and equipment; (c) time consumption and cost; (d) scarce spatial and temporal resolution; and (e) limitations to measure difficult-to-access locations, high flows, and

mountainous rivers with steep slopes (Rantz, 1982; Tauro et al., 2018). It is not, therefore, surprising that a standard worldwide practice is the use of flow stage data to estimate river stream flows. To this aim, a stage-discharge relationship usually called flow rating curve (FRC) is employed (Chow, 1959; Fenton & Keller, 2001). Flow stage data are preferred over other fluvial variables due to their more natural way to be acquired, for instance, by using float gauges or radar technology from infrastructure such as bridges. In this direction, Manfreda (2018) and Manfreda et al. (2020) recently explored a modified version of FRCs suitable for data-scarce environments that enable uncertainty reduction at high flows.

Despite the worldwide efforts of supporting traditional monitoring approaches, many regions present an absence of river gauging stations, leading to a non-uniformly distributed network over the world. The number of standard gauging stations is, in turn, facing a decrease during the last decades due to maintenance difficulties (Crochemore et al., 2020). One possible solution can be the use of technology and novel frameworks, which open new avenues to deal with the current drawbacks of contemporary approaches. For instance, difficult-to-access rivers have nowadays the capacity to be remotely monitored throughout the use of satellite products, fixed cameras, and Unmanned Aerial Systems (UASs) equipped with different sensors.

An explosion in the use of image-based approaches for non-contact river gauging has been reported in the last decade (Leitão, Peña-Haro, Lüthi, Scheidegger, & Moy de Vitry, 2018; Manfreda et al., 2018; Pearce et al., 2020; Perks, Russell, & Large, 2016; Tauro, Pagano, Phamduy, Grimaldi, & Porfiri, 2015). This drive has been likely motivated by the unprecedented increment in technology leading to the improvement of user accessibility (costs and friendly interface) and sensors' performance, including their miniaturization. Large Scale Particle Image Velocimetry (LSPIV) is often used to process images to estimate surface flow velocities in rivers (Fujita, Muste, & Kruger, 1998; Manfreda, Dal Sasso, Pizarro, & Tauro, 2019; Pearce et al., 2020; Strelnikova et al., 2020; Tauro & Salvatori, 2017). However, several other algorithms – adopting alternative approaches – have been developed and currently used for surface flow velocity calculations. Among them, Large-Scale Particle Tracking Velocimetry (LSPTV) (Dal Sasso, Pizarro, Samela, Mita, & Manfreda, 2018), Surface Structure Image Velocimetry (SSIV) (Leitão et al., 2018), Optical Tracking Velocimetry (OTV) (Tauro et al., 2018), Kanade–Lucas Tomasi Image Velocimetry (KLT-IV) (Perks, 2020), and Space–Time Image Velocimetry (STIV) (Fujita, Watanabe, & Tsubaki, 2007). Surface flow velocities can be then converted into river stream flows if the river bathymetry and velocity coefficient are known. River stream flows computed in this way usually are in good agreement with reference values, presenting errors less than 20% (Detert, Johnson, & Weitbrecht, 2017; Dramais, Le Coz, Camenen, & Hauet, 2011; Eltner, Sardemann, & Grundmann, 2020; Huang, Young, & Liu, 2018; Kim et al., 2008; Kinzel & Legleiter, 2019; Le Coz, Hauet, Pierrefeu, Dramais, & Camenen, 2010; Lewis, Lindroth, & Rhoads, 2018). Nevertheless, could there be a way to minimize these errors to make this technology more robust?

Even though the use of these innovative approaches is increasing every year, there are many unanswered questions and uncertainty at real river scales. For instance, what are the guidelines to minimize the errors against stabilization, frame enhancement, post-processing, and transiting features characteristics such as seeding density and clustering of tracers? Unfortunately, only case-specific answers can be given at this regard, opening the interest of many researchers and practitioners to find universal solutions. We have recently shown that tracers characteristics have a critical influence on the accuracy of image velocimetry results (Dal Sasso, Pizarro, & Manfreda, 2020). Indeed, the dynamics on time of seeding density, coefficient of variation of tracers' area, and their spatial distribution in the field of view showed statistical significance on image-based performances. This result motivated us to introduce new metrics to optimize these controlling factors (Pizarro, Dal Sasso, Perks, & Manfreda, 2020a). Based on our experience, the challenge is to identify the temporal window that selects the most informative frames reducing at the same time disturbances and noise. In keeping with this objective, this proof-of-concept paper explores the novel idea of using a reduced number of frames that are catalogued as optimal for the quantification of surface flow velocities and, consequently, river discharge. Only one question is, then, intended to be answered: is it possible to reduce image-based streamflow errors using only a portion of footage catalogued as the best one?

2 | METHODS

2.1 | Field case studies

Two case studies were analysed to illustrate that only a portion of the total number of frames can optimize image-based river discharge estimates. The case studies in question are Murg and La Morge, which are freely available at Perks et al. (2020a, 2020b) – who published a compilation of field case studies for image-based benchmarking purposes.

The first dataset contains measurements performed at the Murg river in Frauenfeld, Switzerland (47.5684 N and 8.8947 E). This field experiment was carried out by Detert et al. (2017) using a DJI Phantom II UAS platform and a GoPro Hero3+ black edition camera, with a resolution of 4096×2160 px. Ten ground control points (GCPs) were distributed in the field of view along both sides of the river to obtain orthorectified images. The calibration factor from pixels to metres was estimated as 0.0156 m/px. Additionally, artificial tracers were deployed onto the water surface from an upstream bridge using wood chips with regular dimensions of 4×4 cm^2. At the moment of acquisition, the cross-sectional area was 4.57 m^2, and the river discharge was 2.76 m^3/s. Reference measurements were acquired in-situ with a Teledyne RDI StreamPro ADCP (Perks et al., 2020a). The same frame rate used by Detert et al. (2017) was adopted in this work, which is three frames per second (fps).

The second case study is located in a 46 km^2 urban catchment in La Morge river, at Voiron, France. On one of the riverbanks, one

analogue Panasonic WV-CP500 camera was mounted on a pole and set at a resolution of 640 × 480 px. The ground sampling distance (GSD) was 0.01 m/px. Corn chips were used to seed the water surface for image-velocimetry purposes artificially, and 48 frames were acquired during approximately 10 s at a frame rate of five fps. The images were converted to greyscale and orthorectified. In order to not modify the flow and camera field of view, reference velocity data were acquired with a mechanical current metre 5 m downstream of the camera measuring location, at 15 locations spaced 0.5 m. These velocity measurements were taken at 20, 60, and 80% of the flow depth. The river discharge was then estimated as 1.32 m^3/s, and the cross-sectional area was 3.41 m^2 (Hauet, 2016).

The Murg and La Morge case studies were pre-processed using binarization to enhance the visibility of tracers to identify and track. Each frame was, therefore, transformed in black (background) and white (tracers) images to reduce the noise due to probable sunlight reflections, poor illumination, and their dynamics over time. To this aim, a binarization threshold was set at 0.70, which corresponds to 70% of 255 (8 bits). Figure 1a presents the location of the case studies as well as an example of the original RGB frame (Figure 1b,c) along with a portion of the pre-processed frame using binarization (Figure 1b′,c′). Table 1 contains the hydraulic data associated to the surveys as well as setting variables for image-based analyses purposes.

2.2 | Image-velocimetry analyses

The Murg case study has a total number of 250 frames at three fps. However, due to some disturbances within frames 50–80 (intrusion of tree branches into the flow field of view), the total used number of frames was restricted to the interval 101–250. La Morge case study was analysed using the 100% of frames available.

LSPIV was carried out employing a command-line version of PIVLab software (Thielicke & Stamhuis, 2014) written by the authors to automate the analysis. The LSPIV algorithm was applied using the Fast Fourier Transform (FFT) with a three-pass standard correlation method (search and interrogation areas of 64 × 32, 32 × 16, and 16 × 8 px). Additionally, the 2 × 3-point Gaussian fit was employed to estimate the sub-pixel displacement peak. LSPIV analyses were iteratively performed using the consecutive sequence style (i.e., 1–2, 2–3, 3–4) and relying on a moving frame window length (FWL) within the total analysed number of frames (i.e., for a fixed FWL, the initial frame was varying). Additionally, the FWL was also increasing in size,

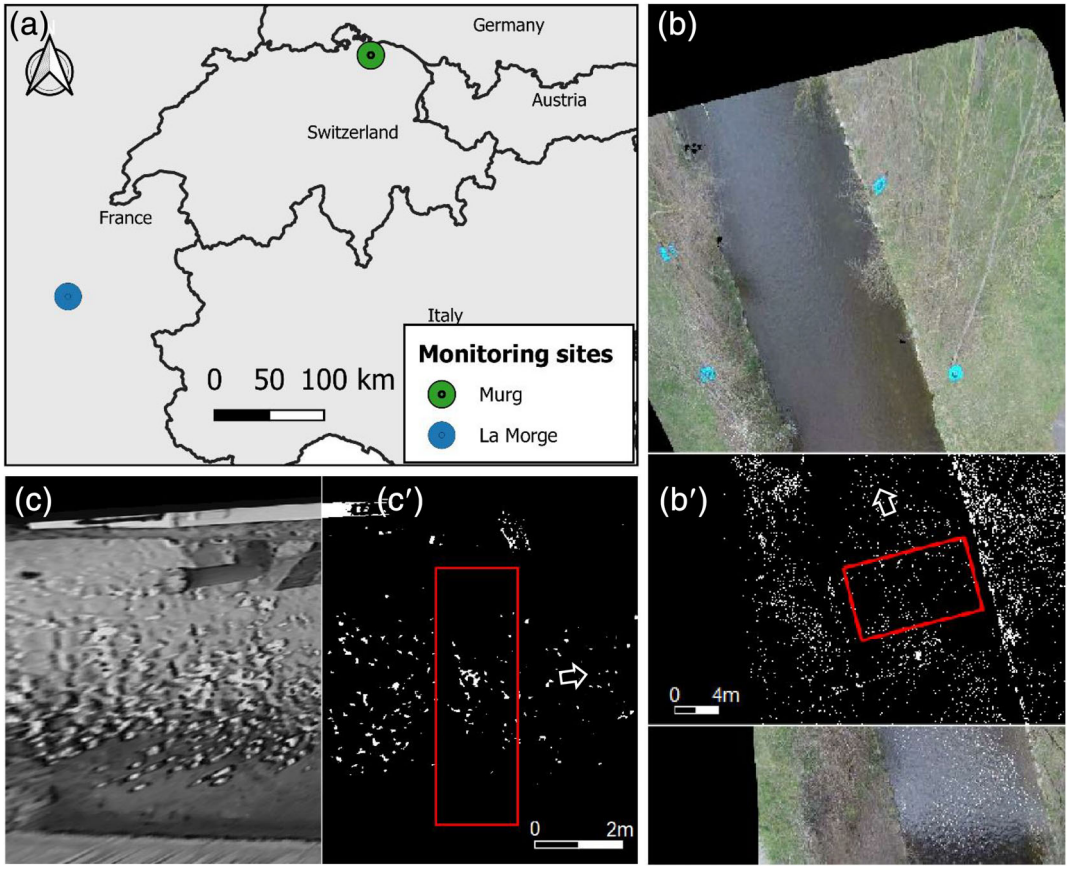

FIGURE 1 Locations of Murg and La Morge monitoring sites (a), illustrating original (b and c) and pre-processed frames (b′ and c′). Red rectangles in (b′ and c′) represent the region of interest, on which the analysis was performed

TABLE 1 Hydraulic information at the moment of the aerial survey at the Murg and La Morge case studies as well as setting variables for analyses purposes

	Hydraulic information				Footage properties and analysis settings				
Case study	Velocity coefficient α	Cross-section area (m^2)	Mean flow velocity (m/s)	Reference discharge (m^3/s)	GSD (m/px)	FPS	Total N° frames	Binarization threshold (%)	FFT 3-passes
Murg	0.78	4.57	0.60	2.76	0.0156	3	150	70	64 × 32
									32 × 16
									16 × 8
La Morge	0.85	3.41	0.39	1.32	0.0100	5	48	70	64 × 32
									32 × 16
									16 × 8

Abbreviations: GSD, ground sampling distance; FFT, fast Fourier transform; FPS, frames per second.

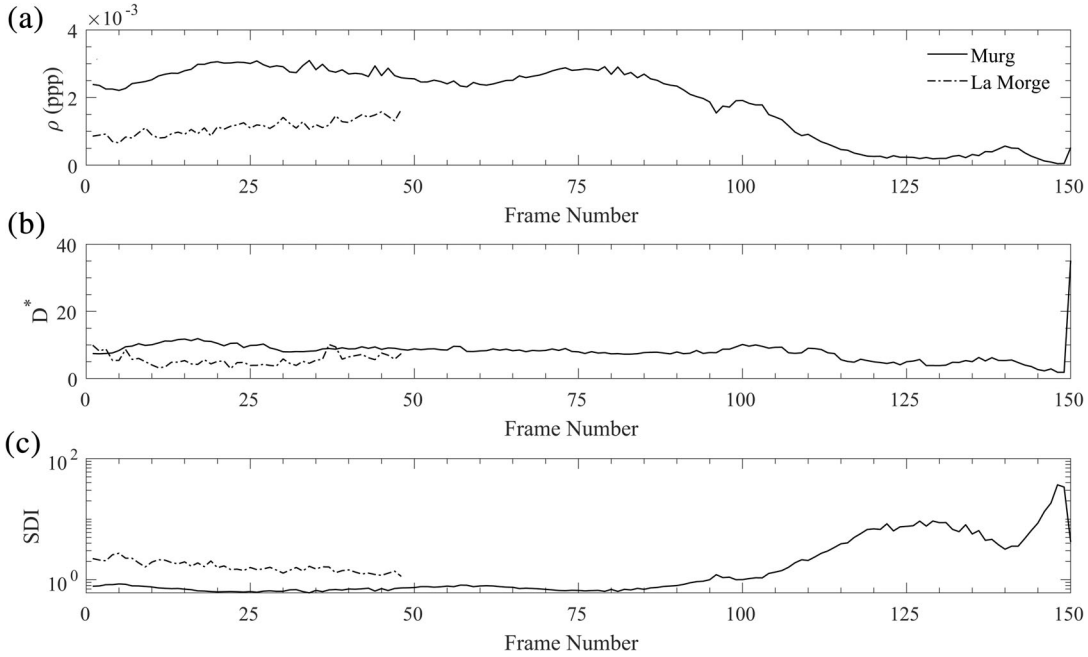

FIGURE 2 Seeding dynamics on a frame-by-frame basis. (a) seeding density (ρ); (b) dimensionless dispersion index (D^*); and (c) SDI as a function of the frame number. Data referring to the Murg is depicted with a continuous line and La Morge with a dashed line

covering all possible cases. These iterative calculations make it possible the characterization of image-velocimetry errors as a function of FWL and its position within the footage duration. LSPIV surface-flow velocity results were averaged and saved within the iterative calculations. No post-processing method was applied to filter spatiotemporal results.

Surface flow velocities were converted to depth-averaged velocities using the velocity coefficient α reported in Table 1 (α is defined as the ratio between depth-averaged velocity and surface flow velocity) (Detert et al., 2017; Eltner et al., 2020). Discharge computation was carried out multiplying the cross-section flow area with the depth-averaged velocity. The performance of LSPIV results was determined by comparing the computed with the reference river discharge. The magnitude of errors was, in consequence, calculated as

$$|\epsilon_Q| = 100 \times \frac{(Q_c - Q_R)}{Q_R}, \quad (1)$$

where Q_C is the computed discharge, Q_R is the reference discharge, and $|\epsilon_Q|$ is the absolute value of errors.

2.3 | Identification of the optimal video window for image velocimetry applications in rivers

Increasing the number of frames within LSPIV analysis has, as a consequence, a systematic reduction of errors generally observed in laboratory flumes (Samarage, Carberry, Hourigan, & Fouras, 2012). This effect is due to temporal averaging, which smooths out outliers and noise with a consequent reduction of errors with the number of

measurements averaged. This latter is possible due to the random nature of outliers, producing a measurement bias with mean value equals zero. It is, therefore, recommended to consider a large number of frames as a general guideline. However, this condition is not always observed in natural environments, where considering a large number of frames leads to increasing the odds of other sources of errors that are not necessarily random. These non-random errors can be related to camera stabilization issues, changes in luminescence and shadows, and features/tracers dynamics on time, among others. In consequence, considering a large number of frames leads to an error reduction expectation but also the introduction of noise of different natures and levels of complexity.

In this regard, Pizarro et al. (2020a) recently introduced the Seeding Distribution Index (SDI) which opens new avenues for identifying the best seeding characteristics for image-velocimetry analysis. SDI is defined as:

$$SDI = D^{*0.1} \Big/ \left(\frac{\rho}{\rho_{cD^*1}}\right), \tag{2}$$

where D^*, ρ, and ρ_{cD^*1} are the empirical spatial clustering level of tracers, the seeding density, and the converging seeding density at the Poisson case ($D^* = 1$), respectively. ρ_{cD^*1} was previously estimated as 1.52E-03 particles per pixel (ppp) in Pizarro et al. (2020a), whereas D^* is computed as $D/D_{Poisson}$ (=[Var(N)/E(N)]/1, where Var(N) and E(N) are the spatial variance and mean value of the number of tracers N computed on subsectors of 60×60 pixels, respectively). Using numerical simulations, Pizarro et al. (2020a) identified a strong positive correlation between SDI and computed errors of image velocimetry applications.

This paper exploits the novel idea of using a combination of the best properties of the concepts mentioned above. Hence, the criteria identifying the best portion of footage to analyze can be summarized as follows: (a) maximization of FWL and (b) minimization of SDI.

3 | RESULTS AND DISCUSSION

Figure 2a,b depict the seeding density and spatial clustering level of tracers on a frame-by-frame basis. The dimensionless SDI index is shown in Figure 2c, revealing an overview of the seeding characteristics for image-based purposes. The curves presented in Figure 2 are representative of single frame analyses, which were performed on the ROI of each frame. The Murg case study is represented by the continuous line, while La Morge with the dashed line.

The Murg case study shows a stable behaviour of ρ and D^* within the first 100 frames, a situation that changes in the final portion of the video. In these final frames, a reduction of ρ and D^* is observed because they also correspond with the final portion of the aerial survey leading to a significant reduction of artificial tracers. This issue is clearly shown in Figure 2c, where SDI shows low and stable performances up to frame number 90 (approximately), from which its values increase. La Morge, alternatively, shows less evident seeding dynamics and therefore, more stability during the video acquisition. However, a slight increase (decrease) in terms of ρ (SDI) is appreciated by increasing the frame number. Lower values of SDI are preferable given their positive correlation with image-based velocity errors.

LSPIV analyses rely on the tracking of features between consecutive frames. This means that the minimum possible FWL is two successive frames. This latter is the minimum for image-based analyses, where velocity estimates are typically spurious because of the absence of temporal averaging. Figure 3 presents $|\epsilon_Q|$ and the averaged-in-2-frames SDI values ($\overline{SDI_2}$) as a function of the initial frame considered for LSPIV analyses. Our findings show that $\overline{SDI_2}$ and

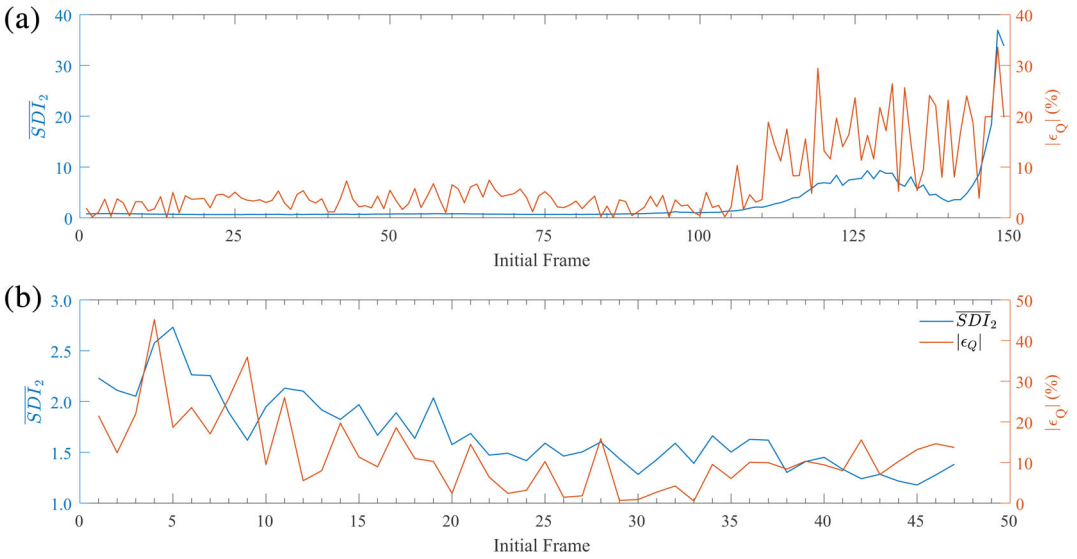

FIGURE 3 $\overline{SDI_2}$ is the averaged SDI using FWL = 2, whereas $|\epsilon_Q|$ is the absolute percentage error. Variables presented as a function of the initial frame considered for LSPIV analysis purposes. (a) Murg, whereas (b) La Morge rivers

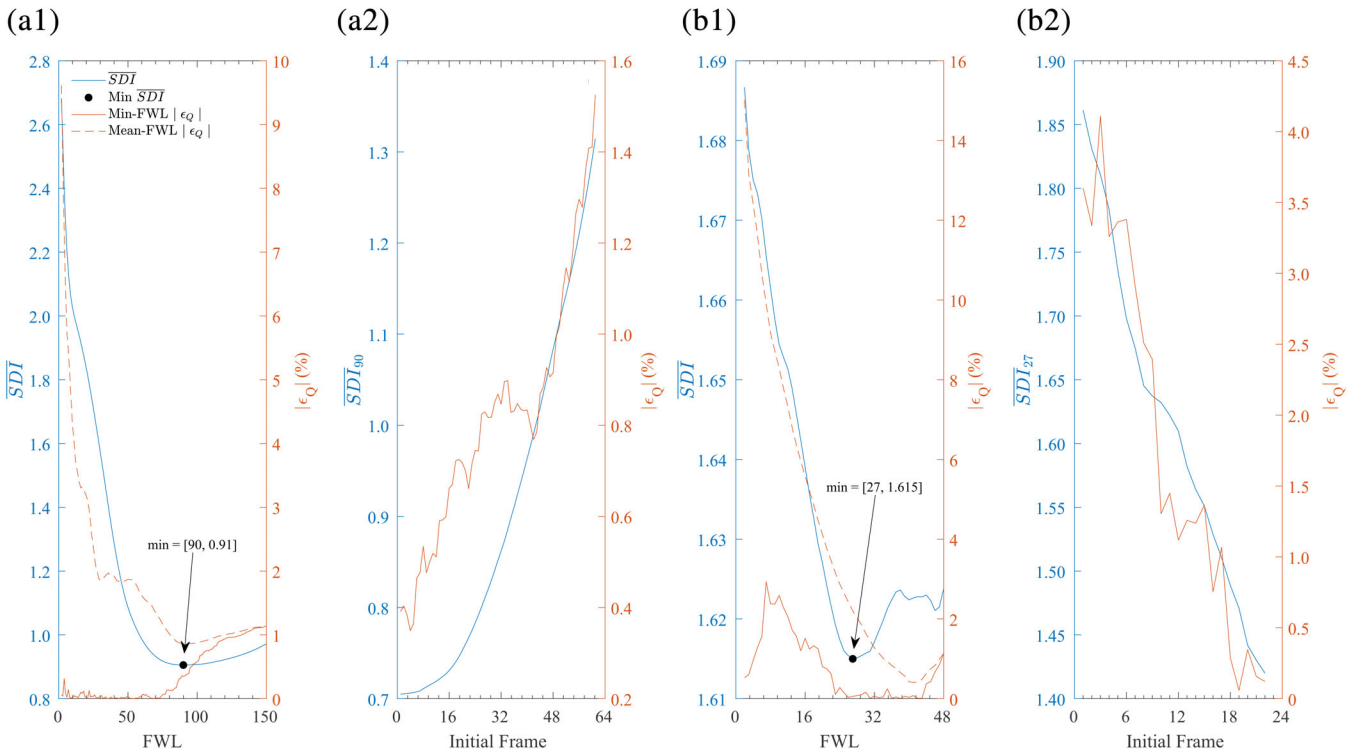

FIGURE 4 $\overline{SDI}$ and $|\epsilon_Q|$ as a function of FWL and its position within the footage duration (initial frame) on (a) Murge and (b) La Morge case studies. Black dots represent the optimal FWL value following the criteria studied in this paper

$|\epsilon_Q|$ are strongly correlated, and the lower the $\overline{SDI_2}$, the lower the $|\epsilon_Q|$. Similar trends are observed on the Murg (Figure 3a) and La Morge (Figure 3b) case studies, having Pearson's coefficients of 0.69 (95% CI: 0.60 to 0.77, $p < .001$) and 0.58 (95% CI: 0.35 to 0.74, $p < .001$), respectively. These results are meaningful because they confirm the findings by Pizarro et al. (2020a) obtained with numerical analyses that highlighted the strong positive correlation between SDI and $|\epsilon_Q|$.

Figure 3 presents errors that are in the range of 0–50%, which are computed using only two consecutive frames. Despite these high values, Figure 3 is useful to illustrate and understand the variability of LSPIV performances within the video duration. Increasing FWL may help to reduce such errors, and accordingly, this issue is analysed more in detail below.

Following this direction, Figure 4 shows a global insight of the averaged $\overline{SDI}$ and $|\epsilon_Q|$ as a function of the FWL and its position characterized by the initial frame considered for analyses. Figure 4a,b refer to Murg and La Morge case studies, respectively. The orange continuous and dashed lines in Figure 4a1,b1 represent the minimum and average $|\epsilon_Q|$ as a function of FWL, which allows image-based performance to be visualized and assessed. Black dots are the optimal cases satisfying the "*footage-best-portion*" criteria investigated in this paper for image-based discharge estimates. Notably, $\overline{SDI}$ and $|\epsilon_Q|$ follow analogous dynamics and the minimum $|\epsilon_Q|$ shows a trend of convergency with the average $|\epsilon_Q|$ for larger FWL values. Additionally, both case studies have only one global minimum $\overline{SDI}$ value at FWL = 90 and 27 – for Murg and La Morge, respectively. Therefore, these FWL values fulfil the criteria adopted in this study.

Figure 4a2,b2 expand the summarized information contained within the black dots. Remarkably, our findings show that the optimal $\overline{SDI}$ ($\overline{SDI_{90}}$ and $\overline{SDI_{27}}$ for Murg and La Morge, respectively) and $|\epsilon_Q|$ have a stronger positive correlation in comparison with $\overline{SDI_2}$ and $|\epsilon_Q|$ (Figure 3). The Pearson's coefficients for the Murg and La Morge case studies are 0.93 (95% CI: 0.89 to 0.96, $p < .001$) and 0.95 (95% CI: 0.88 to 0.98, $p < .001$), respectively. This matter can be visualized in Figure 4a2,b2, also providing evidence of the following trend: the lower the $\overline{SDI_{FWL}}$, the lower $|\epsilon_Q|$. Of particular interest, the minimum errors found adopting the criteria proposed in this study are lower than the ones using the total number of frames available. These errors values are 0.40 versus 1.14% and 0.12 versus 1.13%, respectively.

Figure 5 shows the surface flow velocity maps computed with LSPIV using the optimal FWL. It is important to emphasize that the adopted criteria allowed the definition of an almost complete 2D velocity field without using any type of interpolation. Therefore, the simple and novel idea of using a reduced number of frames – identified as the best ones within the available footage – has been positively tested on the two field case studies selected. This latter opens the possibility of refining image-velocimetry performances for streamflow monitoring, avoiding unnecessary computational burden. The characterization of seeding metrics helped the minimization of errors by correctly identifying the optimal FWL and position within the footage duration. Finally, the framework proposed runs relatively fast, opening up the possibility to be incorporated into fixed cameras, UASs, or smartphones for in-situ image-based analyses.

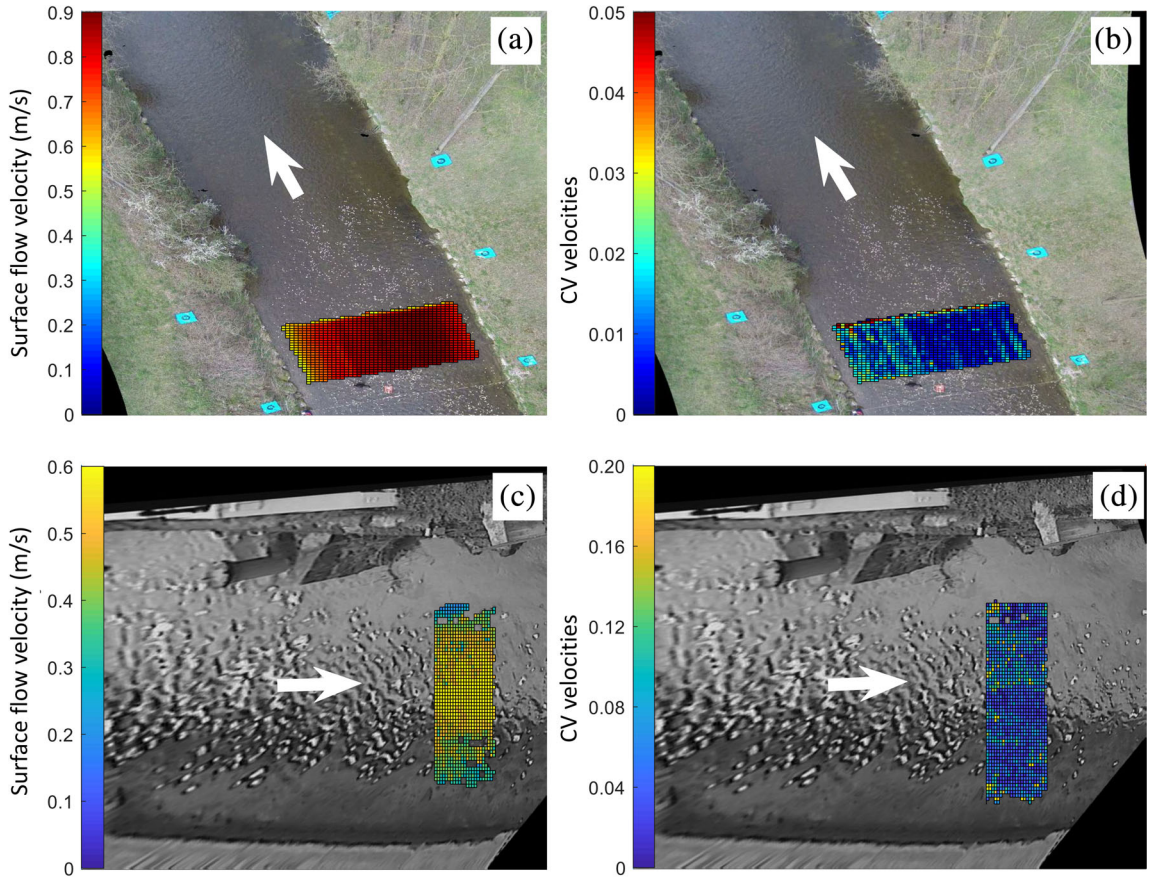

FIGURE 5 Surface flow velocity maps computed with LSPIV using the optimal FWL. CV of velocities using the optimal FWL and different positions within the video. Murge (a) and (b), whereas (c) and (d) La Morge. Arrows represent flow direction

In addition to the flow velocity maps using the optimal FWL, we also computed the flow velocity maps obtained using the same FWL starting from different positions of the video. This produced an ensemble of velocities that differ from the optimal one. An estimate of the stability of the image velocimetry performances is summarized in Figures 5b,d, where the coefficient of variation (CV) of these velocities is depicted. It can be noticed that the deviations from optimal configurations display a spatial pattern that may undoubtedly be influenced by the distribution seedings. Based on the evidence of these graphs, a higher variability is observed in the portion of the cross-section where lower flow velocities are observed. This is interesting evidence that deserves to be further investigated to improve the quality of these techniques not only at the scale of the cross-section (or scene) but also at the local scale.

4 | STRENGTHS AND LIMITATIONS

One of the main strengths of this study was the minimization of LSPIV errors for river streamflow monitoring, avoiding any post-processing procedures to remove spurious results. Additionally, the Murg and La Morge case studies – freely available at Perks et al. (2020a, 2020b) – were considered for testing the reliability of the method. This method can be particularly useful for fixed LSPIV stations aimed at continuous monitoring of river discharge, allowing memory space requirements of experimental systems to be minimized. As a general remark, the method relies on the positive correlation between SDI and image velocimetry errors. Therefore, the correct identification of the optimal FWL is influenced by the temporal and spatial variability of seedings. The larger is the variability of these features the simpler is to identify optimal FWL. We must acknowledge that only two case studies were included, although promising, further investigations on additional field studies or numerical simulations should be carried out to generalize the obtained findings. Furthermore, the case studies were artificially seeded to simplify the identification of moving patterns on the water surface. This latter helped the identification and tracking of the transiting features through image-velocimetry analyses. Finally, LSPIV was set to run using FFT with a three-pass standard correlation method only.

5 | CONCLUSION

In this paper, we investigated the performances of LSPIV for streamflow estimates. To this aim, we adopted the new dimensionless SDI index that combines seeding metrics for image-based analyses. A

novel approach was introduced, relying on the idea of using a reduced number of frames that are catalogued as the "*optimal*" ones within the footage length. To select the best portion of footage to analyse, two criteria were explored: (a) the maximization of the number of frames used in the analysis, subject to (b) the minimization of SDI. The Murg and La Morge field case studies (located in Switzerland and France, respectively) were considered as a proof-of-concept of the proposed framework. Seeding density, clustering level of tracers, and SDI were empirically estimated on a frame-by-frame basis. Our results support the idea of choosing a reduced part of footage can enable the reduction of image-velocimetry errors in rivers. In particular, the computed river discharge error at the optimal portion of the footage was about 0.40% and 0.12%, lower than considering all frames available. The authors are keen to apply these ideas to a larger dataset under different field and environmental conditions, countries, dates, personnel involved, and footage information.

ACKNOWLEDGEMENTS

This work was supported by the COST Action CA16219 "HARMONIOUS—Harmonization of UAS techniques for agricultural and natural ecosystems monitoring."

CODE AVAILABILITY STATEMENT

The code used to compute the SDI index as well as seeding metrics is available at https://doi.org/10.17605/OSF.IO/8EGQW (Pizarro et al., 2020b).

DATA AVAILABILITY STATEMENT

The data that support the findings of this study are openly available in 4TU.Centre for Research Data at https://doi.org/10.4121/uuid:014d56f7-06dd-49ad-a48c-2282ab10428e (Perks, Sasso, et al., 2020).

ORCID

Alonso Pizarro https://orcid.org/0000-0002-7242-6559
Silvano Fortunato Dal Sasso https://orcid.org/0000-0003-1376-7764
Salvatore Manfreda https://orcid.org/0000-0002-0225-144X

REFERENCES

Chow, V. T. (1959). Open-channel hydraulics. In *Open-channel hydraulics*. New York: McGraw-Hill.

Crochemore, L., Isberg, K., Pimentel, R., Pineda, L., Hasan, A., & Arheimer, B. (2020). Lessons learnt from checking the quality of openly accessible river flow data worldwide. *Hydrological Sciences Journal*, *65*, 699–711. https://doi.org/10.1080/02626667.2019.1659509

Dal Sasso, S. F., Pizarro, A., & Manfreda, S. (2020). Metrics for the quantification of seeding characteristics to enhance image velocimetry performance in rivers. *Remote Sensing*, *12*. https://doi.org/10.3390/rs12111789

Dal Sasso, S. F., Pizarro, A., Samela, C., Mita, L., & Manfreda, S. (2018). Exploring the optimal experimental setup for surface flow velocity measurements using PTV. *Environmental Monitoring and Assessment*, *190*(8), 460. https://doi.org/10.1007/s10661-018-6848-3

Detert, M., Johnson, E. D., & Weitbrecht, V. (2017). Proof-of-concept for low-cost and non-contact synoptic airborne river flow measurements. *International Journal of Remote Sensing*, *38*, 2780–2807. https://doi.org/10.1080/01431161.2017.1294782

Dramais, G., Le Coz, J., Camenen, B., & Hauet, A. (2011). Advantages of a mobile LSPIV method for measuring flood discharges and improving stage-discharge curves. *Journal of Hydro-Environment Research*, *5*, 301–312. https://doi.org/10.1016/j.jher.2010.12.005

Eltner, A., Sardemann, H., & Grundmann, J. (2020). Technical note: Flow velocity and discharge measurement in rivers using terrestrial and unmanned-aerial-vehicle imagery. *Hydrology and Earth System Sciences*, *24*(3), 1429–1445. https://doi.org/10.5194/hess-24-1429-2020

Fenton, J. D., & Keller, R. J. (2001). *The Calculation of Streamflow from Measurements of Stage*. Clayton, Victoria: Cooperatiive Research Center for Catchment Hydrology.

Fujita, I., Muste, M., & Kruger, A. (1998). Large-scale particle image velocimetry for flow analysis in hydraulic engineering applications. *Journal of Hydraulic Research*, *36*, 397–414. https://doi.org/10.1080/00221689809498626

Fujita, I., Watanabe, H., & Tsubaki, R. (2007). Development of a non-intrusive and efficient flow monitoring technique: The space-time image velocimetry (STIV). *International Journal of River Basin Management*, *5*, 105–114. https://doi.org/10.1080/15715124.2007.9635310

Hauet, A. (2016). Monitoring river flood using fixed image-based stations: Experience feedback from 3 rivers in France. Paper presented at: *River Flow - Proceedings of the International Conference on Fluvial Hydraulics, RIVER FLOW 2016*. https://doi.org/10.1201/9781315644479-87

Huang, W. C., Young, C. C., & Liu, W. C. (2018). Application of an automated discharge imaging system and LSPIV during typhoon events in Taiwan. *Water (Switzerland)*, *10*. https://doi.org/10.3390/w10030280

Kim, Y., Muste, M., Hauet, A., Krajewski, W. F., Kruger, A., & Bradley, A. (2008). Stream discharge using mobile large-scale particle image velocimetry: A proof of concept. *Water Resources Research*, *44*(9), W09502. https://doi.org/10.1029/2006WR005441

Kinzel, P. J., & Legleiter, C. J. (2019). sUAS-based remote sensing of river discharge using thermal particle image velocimetry and bathymetric Lidar. *Remote Sensing*, *11*(19), 2317.

Le Coz, J., Hauet, A., Pierrefeu, G., Dramais, G., & Camenen, B. (2010). Performance of image-based velocimetry (LSPIV) applied to flash-flood discharge measurements in Mediterranean rivers. *Journal of Hydrology*, *394*(1), 42–52.

Leitão, J. P., Peña-Haro, S., Lüthi, B., Scheidegger, A., & Moy de Vitry, M. (2018). Urban overland runoff velocity measurement with consumer-grade surveillance cameras and surface structure image velocimetry. *Journal of Hydrology*, *565*, 791–804. https://doi.org/10.1016/j.jhydrol.2018.09.001

Lewis, Q. W., Lindroth, E. M., & Rhoads, B. L. (2018). Integrating unmanned aerial systems and LSPIV for rapid, cost-effective stream gauging. *Journal of Hydrology*, *560*, 230–246. https://doi.org/10.1016/j.jhydrol.2018.03.008

Manfreda, S. (2018). On the derivation of flow rating curves in data-scarce environments. *Journal of Hydrology*, *562*, 151–154. https://doi.org/10.1016/j.jhydrol.2018.04.058

Manfreda, S., Dal Sasso, S. F., Pizarro, A., & Tauro, F. (2019). New insights offered by UAS for river monitoring. In *Applications of small unmanned aircraft systems: Best practices and case studies*. Boca Raton, FL.

Manfreda, S., Link, O., & Pizarro, A. (2018). A theoretically derived probability distribution of scour. *Water (Switzerland)*, *10*. https://doi.org/10.3390/w10111520

Manfreda, S., McCabe, M. F., Miller, P. E., Lucas, R., Madrigal, V. P., Mallinis, G., … Toth, B. (2018). On the use of unmanned aerial systems for environmental monitoring. *Remote Sensing*, *10*. https://doi.org/10.3390/rs10040641

Manfreda, S., Pizarro, A., Moramarco, T., Cimorelli, L., Pianese, D., & Barbetta, S. (2020). Potential advantages of flow-area rating curves compared to classic stage-discharge-relations. *Journal of Hydrology*, *585*, 124752.

Owe, M. (1985). Long-term streamflow observations in relation to basin development. *Journal of Hydrology*, *78*(3-4), 243–260.

Pearce, S., Ljubičić, R., Peña-Haro, S., Perks, M., Tauro, F., Pizarro, A., … Manfreda, S. (2020). An evaluation of image velocimetry techniques under low flow conditions and high seeding densities using unmanned aerial systems. *Remote Sensing*, *12*. https://doi.org/10.3390/rs12020232

Perks, M., Dal Sasso, S. F., Detert, M., Hauet, A., Jamieson, E., Le Coz, J., … Manfreda, S. (2020b). Data on the harmonization of image velocimetry techniques, from seven different countries. 4TU. Research Data. Dataset. https://doi.org/10.4121/uuid:014d56f7-06dd-49ad-a48c-2282ab10428e

Perks, M. T. (2020). KLT-IV v1. 0: Image velocimetry software for use with fixed and mobile platforms. Geoscientific Model Development Discussions: pp. 1–27.

Perks, M. T., Dal Sasso, S. F., Hauet, A., Jamieson, E., Le Coz, J., Pearce, S., … Manfreda, S. (2020a). Towards harmonisation of image velocimetry techniques for river surface velocity observations. *Earth System Science Data*, *12*(3), 1545–1559. https://doi.org/10.5194/essd-12-1545-2020

Perks, M. T., Russell, A. J., & Large, A. R. G. (2016). Technical note: Advances in flash flood monitoring using unmanned aerial vehicles (UAVs). *Hydrology and Earth System Sciences*, *20*, 4005–4015. https://doi.org/10.5194/hess-20-4005-2016

Pizarro, A., Dal Sasso, S. F., Perks, M. T., & Manfreda, S. (2020a). Spatial distribution of tracers for optical sensing of stream surface flow. *Hydrology and Earth System Sciences*. https://doi.org/10.5194/hess-2020-188

Pizarro A, Dal Sasso SF, Perks MT, Manfreda S. (2020b). Identifying the optimal spatial distribution of tracers for optical sensing of stream surface flow (Version 0.1). *[codes] OSF*. https://doi.org/10.17605/OSF.IO/8EGQW

Rantz, S. E. (1982). *Measurement and computation of streamflow*. Washington: US Department of the Interior, Geological Survey.

Rehmel, M. (2007). Application of acoustic doppler velocimeters for streamflow measurements. *Journal of Hydraulic Engineering*, *133*, 1433–1438. https://doi.org/10.1061/(ASCE)0733-9429(2007)133:12(1433)

Samarage, C. R., Carberry, J., Hourigan, K., & Fouras, A. (2012). Optimisation of temporal averaging processes in PIV. *Experiments in Fluids*, *52*, 617–631. https://doi.org/10.1007/s00348-011-1080-8

Strelnikova, D., Paulus, G., Käfer, S., Anders, K.-H., Mayr, P., Mader, H., … Schneeberger, R. (2020). Drone-based optical measurements of heterogeneous surface velocity fields around fish passages at hydropower dams. *Remote Sensing*, *12*, 384. https://doi.org/10.3390/rs12030384

Tauro, F., Pagano, C., Phamduy, P., Grimaldi, S., & Porfiri, M. (2015). Large-scale particle image velocimetry from an unmanned aerial vehicle. *IEEE/ASME Transactions on Mechatronics*, *20*(6), 3269–3275.

Tauro, F., & Salvatori, S. (2017). Surface flows from images: Ten days of observations from the Tiber River gauge-cam station. *Hydrology Research*, *48*, 646–655. https://doi.org/10.2166/nh.2016.302

Tauro, F., Selker, J., Van De Giesen, N., Abrate, T., Uijlenhoet, R., Porfiri, M., et al. (2018). Measurements and observations in the XXI century (MOXXI): Innovation and multi-disciplinarity to sense the hydrological cycle. *Hydrological Sciences Journal*, *63*, 169–196. https://doi.org/10.1080/02626667.2017.1420191

Tauro, F., Tosi, F., Mattoccia, S., Toth, E., Piscopia, R., & Grimaldi, S. (2018). Optical tracking velocimetry (OTV): Leveraging optical flow and trajectory-based filtering for surface streamflow observations. *Remote Sensing*, *10*(12). https://doi.org/10.3390/rs10122010

Tazioli, A. (2011). Experimental methods for river discharge measurements: Comparison among tracers and current meter. *Hydrological Sciences Journal*, *56*(7), 1314–1324.

Thielicke, W., & Stamhuis, E. J. (2014). PIVlab – Towards user-friendly, affordable and accurate digital particle image velocimetry in MATLAB. *Journal of Open Research Software*, *2*, e30. https://doi.org/10.5334/jors.bl

WMO (2010). Computation of discharge. In *Manual on stream gauging* (Vol. 2), Geneva, Switzerland: World Meteorological Organization.

Yorke, T. H., & Oberg, K. A. (2002). Measuring river velocity and discharge with acoustic Doppler profilers. *Flow Measurement and Instrumentation*, *13*(5), 191–195.

How to cite this article: Pizarro A, Dal Sasso SF, Manfreda S. Refining image-velocimetry performances for streamflow monitoring: Seeding metrics to errors minimization. *Hydrological Processes*. 2020;34:5167–5175. https://doi.org/10.1002/hyp.13919